INSTITUTE OF PHYSICS PUBLISHING JOURNAL OF MICROMECHANICS AND MICROENGINEERING

J. Micromech. Microeng. **14** (2004) S17–S22 PII: S0960-1317(04)77943-7

New tunable RF MEMS microinductors design

Charles-Marie Tassetti[1], **Gaëlle Lissorgues**[1] **and Jean-Paul Gilles**[2]

[1] ESYCOM-EA2552, Groupe ESIEE, Cité Descartes, 93162 Noisy-le-Grand, France
[2] IEF, UMR8622 CNRS, University of Paris XI, 91405 Orsay, France

E-mail: tassettc@esiee.fr, g.lissorgues@esiee.fr and jean-paul.gilles@ief.u-psud.fr

Received 18 March 2004
Published 20 August 2004
Online at stacks.iop.org/JMM/14/S17
doi:10.1088/0960-1317/14/9/003

Abstract
This paper outlines the capabilities of RF MEMS tunable microinductors designed using mechanical displacements that change the magnetic coupling coefficient between circuits. The design and fabrication of a first and an optimized second tunable microinductor prototype are presented. We report a 50% inductance variation from 1.5 to 5 GHz measured on the first test wafers. Moreover, these tunable inductors, which have continuous variations, can be integrated with tunable capacitors into reconfigurable RF systems suitable for future wideband RF communications. The design of basic functions, such as a simple phase shifter cell or a tunable impedance, is lastly described.

1. Introduction

Early research on RF MEMS focused on switches or tunable capacitors. These technologies are nowadays suitable for designing systems such as high-performance n-bit phase shifters or simple filters. RF MEMS switches and tunable capacitors are key components for the next generation of communication systems such as analog software radio.

Other specific applications, such as true time delay lines or tunable RF filtering, could also require tunable inductors to avoid mismatching [1]. A delay line using both tunable capacitors and tunable inductors maintains the characteristic impedance constant while the delay can be changed. Therefore the tunable inductor is also an enabling technology.

Some papers discuss the design and fabrication of tunable microinductors, using magnetic materials or mechanical displacements. Circuit inductance increases with the effective permeability of the surrounding environment. Some magnetic materials can be driven by a small dc magnetic field applied in their hard direction, resulting in a permeability variation [2]. Our work is to design tunable microinductors for microwave communication systems. For this frequency range, over 1 GHz, most magnetic materials become non-magnetic, with relative permeability $\mu_r = 1$. These materials are unsuitable for our applications. The recent generation of tunable inductors also shows that discrete variations have been obtained using switched microinductors, with performance primarily dependent on the switches [3]. Continuous variations have also been observed either working on the geometry and/or the coupling coefficient [4]. To date, none of the published tunable microinductors fit our specifications (high variation ratio, high frequency range applications). Therefore, to achieve inductors with high variation ratio and continuous variations at microwave frequencies, we decided to focus on magnetic coupling between circuits [5]. In the first part, this paper presents the design, the fabrication and the measurements of different kinds of microinductors. Then two key RF building block functions, a simple phase shifter and a tunable impedance, are presented.

2. Design of the tunable microinductor

A tunable microinductor can be designed by controlling the magnetic coupling coefficient between two different circuits. When two similar inductors L_0 are very close to one another, the mutual inductor is defined by $M = kL_0$, with a coupling factor k. These inductors can be connected in series or in parallel while the current flows in two adjacent lines can have same or opposite directions. If the current flows have the same direction, M is positive, else M is negative. In theory, the coupling factor k can take any value between 0 and 1. The theoretical variation ratios in all configurations are shown

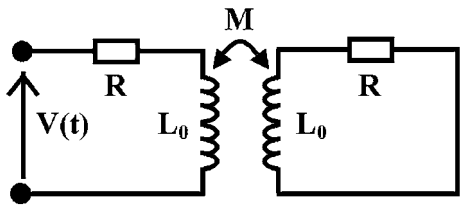

Figure 1. Transformer equivalent circuit.

Table 1. Summary of all possible configurations.

Association	Flow direction	L_{TOT}	Ratio
Series	Same	$2L_0(1+k)$	$(1+k_{max})/(1+k_{min})$
Parallel	Same	$L_0(1+k)/2$	$(1+k_{max})/(1+k_{min})$
Series	Opposite	$2L_0(1-k)$	$(1-k_{min})/(1-k_{max})$
Parallel	Opposite	$L_0(1-k)/2$	$(1-k_{min})/(1-k_{max})$

in table 1. Very large tuning ratios can be expected with opposite current flows. But connections between lines are technologically complex and introduce parasitic elements, in particular small constant parasitic inductances. Nevertheless, it is possible to reach good variation ratios with a simple transformer configuration.

2.1. Configuration of the transformer

In this configuration, the transformer primary circuit represents the microinductor. The secondary circuit is short circuited: it is a loop of the same dimensions as the primary inductor (figure 1). Moreover, there is no electrical connection between these two circuits, which reduces parasitic effects.

The two circuits are separated by a dielectric gap of a few μm and are magnetically coupled by the coupling coefficient k. These two circuits have the same dimensions, so that they present the same equivalent circuit, which is a series association (L_0, R). As we have coupling coefficient k between the two circuits, the equivalent impedance of the primary becomes (1):

$$Z_{eq} = (R + jL_0\omega) + \frac{(kL_0\omega)^2}{(R + jL_0\omega)}. \quad (1)$$

The imaginary part of the equivalent impedance represents the equivalent inductance (2), and the equivalent resistance is extracted from the real part (3):

$$L_{eq} = L_0\left(1 - \frac{(kL_0\omega)^2}{R^2 + (L_0\omega)^2}\right) \quad (2)$$

$$R_{eq} = R\left(1 + \frac{(kL_0\omega)^2}{R^2 + (L_0\omega)^2}\right). \quad (3)$$

2.2. Circuit analysis

As shown in table 2, this system exhibits two main behaviors. Inductance becomes constant at high frequencies depending on the coupling coefficient. In our design, the tunable inductor is realized by controlling the gap between the two circuits. The transformer secondary circuit, the loop, is patterned on a movable silicon cantilever, which represents the mechanical part of the structure. This cantilever bends under the electrostatic pressure produced by an electrostatic actuator. The distance between the two circuits is then reduced and the magnetic coupling coefficient increases, resulting in an inductance variation. As a consequence, the more the coupling coefficient increases, the more the inductance decreases, and unfortunately the more the resistance increases. Figure 2 shows the evolution of the equivalent inductance as a function of the frequency for different coupling coefficients, using $L_0 = 2.2$ nH, $R = 2\Omega$.

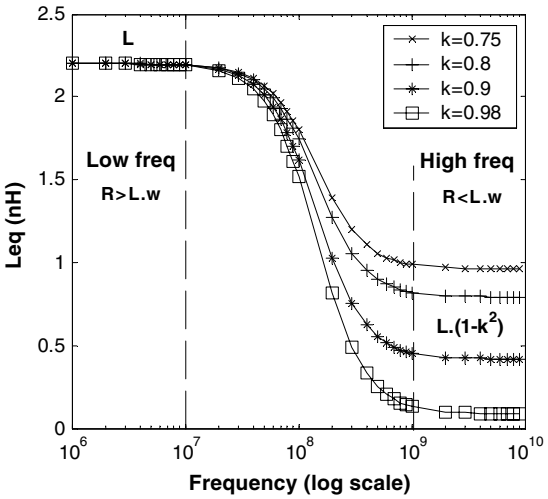

Figure 2. Inductance variation for different coupling coefficients k.

Table 2. Frequency domains in the transformer configuration.

Low frequencies	High frequencies
$R \gg L_0\omega$	$L_0\omega \gg R$
$L_{eq} \approx L_0\left[1 - \left(\frac{kL_0\omega}{R}\right)^2\right]$	$L_{eq} \approx L_0(1-k^2)$
$R_{eq} \approx R\left[1 + \left(\frac{kL_0\omega}{R}\right)^2\right]$	$R_{eq} \approx R(1+k^2)$

Since $0 < k_{min} < k_{max} < 1$, where k_{min} and k_{max} represent respectively the minimum and the maximum coupling coefficients, the variation ratio expression (4) is

$$\text{Variation} = \frac{1 - k_{min}^2}{1 - k_{max}^2}. \quad (4)$$

For example, if $k_{min} = 0.7$ and $k_{max} = 0.95$, the variation ratio of the transformer structure is 5.2 as the maximal variation ratio of table 1 is 6. Nevertheless, the transformer design appears to be the most efficient structure in the trade-off between inductance variation and technological process.

3. Fabrication

3.1. Process description

This tunable inductor is processed using two different wafers: an SOI wafer for mechanical parts and a glass wafer. Seven masking levels are required for this process. The starting substrate is a 4 inch glass wafer (figure 3). An air cavity is obtained using HF wet etching. A metallic layer is deposited and patterned to create the microinductor, pads for measurement probes and the first part of actuation electrodes.

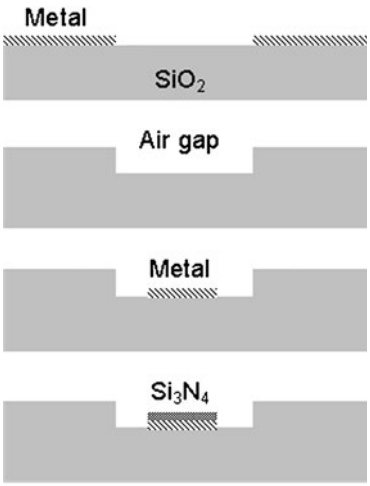

Figure 3. Glass wafer process.

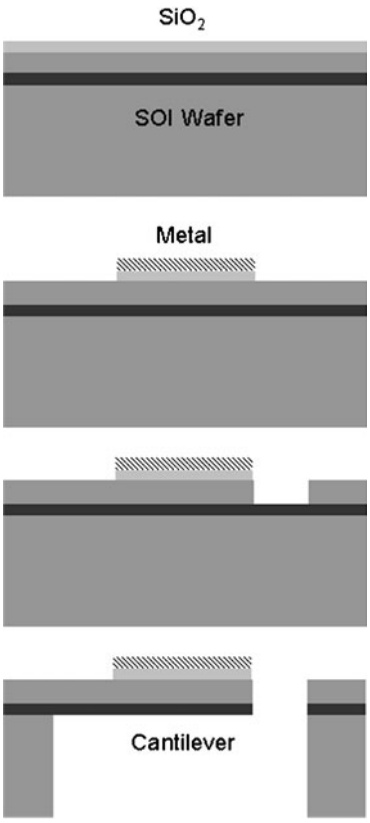

Figure 4. SOI wafer process.

The microinductor and the first electrode are covered by silicon nitride overlay deposited using plasma-enhanced chemical vapor deposition (PECVD). Silicon nitride is etched by reactive ion etching (RIE).

The second substrate is a 4 inch SOI wafer with a 15 μm thick silicon layer on a 2 μm thick silicon dioxide layer (figure 4). The growth of a thermal oxide is followed by a metal deposition. This layer is patterned to design the loop and the second part of the actuation electrodes. The loop and the electrodes can be also covered by silicon nitride

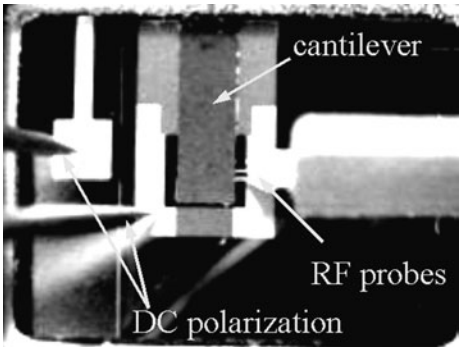

Figure 5. First prototype of tunable microinductor.

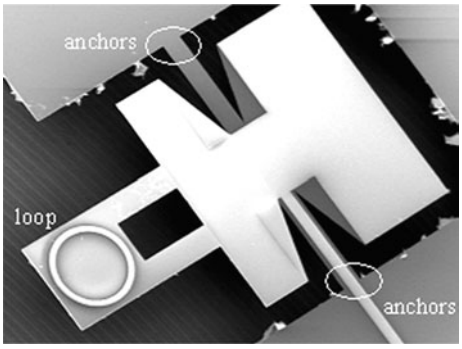

Figure 6. Second prototype of tunable microinductor.

overlay deposited using PECVD. The top side is first etched by deep reactive ion etching (DRIE) and the cantilever is then released by another DRIE on the backside. Silicon dioxide is etched by RIE. Lastly, wafers are aligned and bonded by anodic bonding at low temperature, which is not a standard condition. The main technological difficulty lies in the anodic bonding process as it requires high polarization voltage, consequently creating sticking problems.

3.2. The different prototypes

As seen in the first paragraph, the inductance variation relies on mechanical displacements. Therefore to reach high variation ratios we need large mechanical displacements between the microinductor and the loop. Electrostatic actuation is the easiest way to achieve mechanical displacements, however large displacements require high voltage. The first structures present a 15 μm gap and 150 V pull-in voltage (figure 5), resulting in a measured ratio around 2.

A new mechanical structure (figure 6), has been designed to increase the variation ratio. The displacements are improved using flexion and torsion bars. In order to also reduce the pull-in voltage to 60 V, the structure's dimensions have been determined by analytic solution, and electro/mechanical finite element analysis. The simulated maximum displacement between the two circuits is higher than 30 μm, resulting in an expected inductance variation ratio of 4. Improvements are still necessary to overcome stress troubles in mechanical parts in order to release flat structures, which can be achieved by modifying some technological parameters.

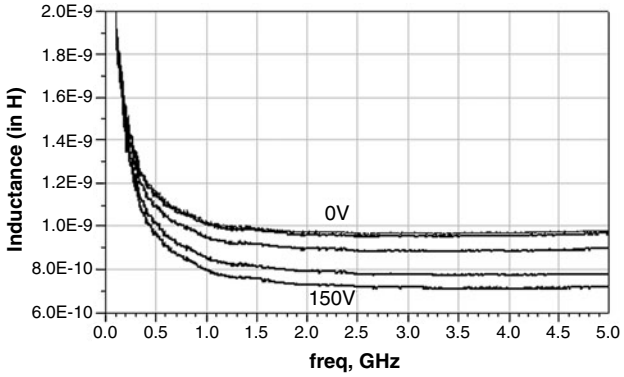

Figure 7. Plot of the inductance variation for structure (c) with actuation voltage from 0 to 150 V.

Table 3. First prototype: structures tested.

	Micro-inductor diameter (in μm)	Structure on cantilever
(a)	800	800 μm × 800 μm square
(b)	800	Nothing
(c)	800	800 μm loop
(d)	600	600 μm loop

4. Measurements

4.1. Measurement setup and results

The microwave on-wafer test measurement setup is an Agilent 8722ES vector network analyzer using ground-signal-ground probes with a 150 μm pitch, performed between 0.1 and 5 GHz. With one port of the inductor being grounded, reflection measurements are performed (S_{11} parameter). We need two more probes for dc actuation: the first one is connected to the RF ground line and the second one to the cantilever electrode pad (figure 5). We measured the first structures at different actuation voltages, from 0 V to 150 V, which is the cantilever pull-in voltage. We made measurements on four different structures: two reference structures, and two test structures (table 3). All the micro-inductors and loops are 1 turn 50 μm track width inductors. As reference structures, we used an 800 μm diameter microinductor associated with a silicon cantilever without a loop, and one with a metal layer. The high-resistivity silicon cantilever has little influence on the inductance value. For low frequencies, the resistor impedance is prevailing, so we have an inductance value which is frequency dependent. At higher frequencies, the inductor impedance is greater than the resistor impedance and the inductance value becomes constant (table 2 and figure 7). Extracted inductance values demonstrate that we can reach very high variation ratios by optimizing our tunable microinductor design. The air gap between the microinductor and the loop is 15 μm at 0 V actuation. From 1 GHz to 5 GHz, structure (c) has a 0.97 nH microinductor at 0 V and 0.71 nH at 150 V, resulting in a 36% variation ratio. Structure (d) presents the highest variation ratio reaching 50%: 0.65 nH at 150 V against 1 nH at 0 V. Without a cantilever, 800 μm and 600 μm diameter microinductors have inductance values of 2.2 nH and 1.8 nH, respectively. The inductance of the 800 μm diameter first tunable structure becomes almost

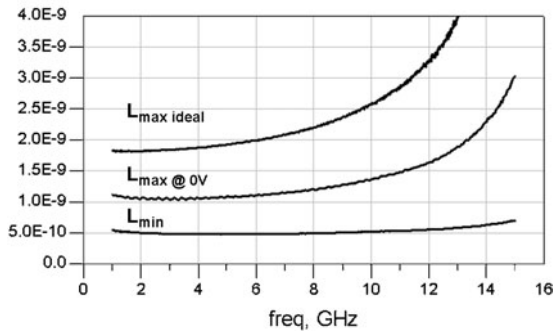

Figure 8. Inductance value extracted from the second prototype.

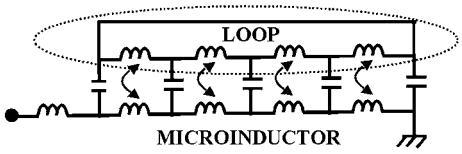

Figure 9. Compact lumped element model.

constant over the frequency range of 1–5 GHz. The inductance between 2.5 GHz and 5 GHz (5), as a function of the actuation voltage, is extracted from the measurements:

$$L_{eq}(V) = 0.97 - 3.68 \times 10^{-5}V + 2.57 \times 10^{-6}V^2 - 1.125 \times 10^{-7}V^3 \quad \text{(in nH)}. \tag{5}$$

For the second prototype (figure 6), on-wafer measurements have been performed for three different configurations (figure 8) from 1 GHz to 15 GHz:

- a 800 μm diameter inductor alone, which represents the ideal maximal inductance value ($L_{max\ ideal}$);
- the same inductor with the loop and the mechanical part at the pull-in voltage, which is the minimal inductance value (L_{min});
- the same inductor with the loop and the mechanical part at 0 V actuation voltage, which is our real maximal inductance value (L_{max} at 0 V).

Note that the inductance value of the tunable inductor at 0 V actuation voltage is smaller than the maximal inductance value this structure can reach. Because the movable parts of the realized structures bent under mechanical stress, the maximal air gap between the inductor and the loop at 0 V is reduced. L at 0 V is therefore underestimated in this instance.

4.2. Equivalent circuit

We built an equivalent circuit based on the design geometry (figure 9). Elements of this model can be evaluated by classical equations: both the inductance and the coupling factor are computed using a magnetic flow method. Wire thickness is less than the skin depth at 5 GHz, therefore wire resistance is closed to dc resistance, and the capacitance between the inductor and the loop is approximated by the 'parallel-plates formula'.

Wire resistance is set inside each inductor element. In figure 9, upper inductors represent the loop, and lower inductors the microinductor. We only consider magnetic

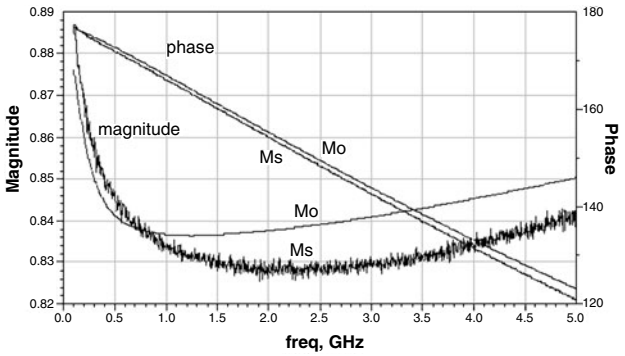

Figure 10. Measured inductance versus equivalent circuit inductance (Mo: model, Ms: measurements).

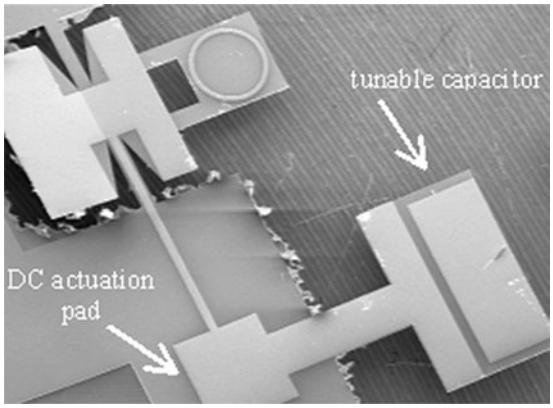

Figure 11. Series association of a tunable inductor and a tunable capacitor, mechanical part only (SEM view).

coupling between two adjacent wires; all other coupling coefficients are neglected. The equivalent circuit for structure (c) at 0 V is $R = 0.72\ \Omega$, $L = 0.51$ nH, $C = 0.1$ pF and $k = 0.84$ for each branch. This compact lumped element model gives results in good agreement with measurements (figure 10). Since the magnitude curves have a small range value, from 0.83 to 0.89, the measured magnitude appears very noisy. The measured phase is also noisy but the scale value is higher.

5. Tunable RF systems

5.1. Design

We decided to use this tunable inductor to design tunable RF basic functions, which is the first step in the conception of future reconfigurable wideband systems. The first system is a simple series association of one tunable inductor and one basic metal–air–metal (MAM) tunable capacitor (figure 11). This tunable impedance presents either a capacitive behavior or an inductive behavior, depending on the applied actuation voltages. The integration of the different components on the same wafer is performed using the same technological process for both inductors and capacitors. The components are connected by CPW patterned on the glass wafer.

The second system realized is a tunable phase shifter based on the simple π high-pass cell (figure 12). This design is

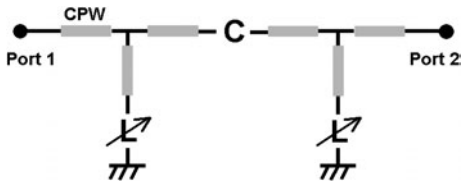

Figure 12. Schematic circuit of the π cell tunable phase shifter.

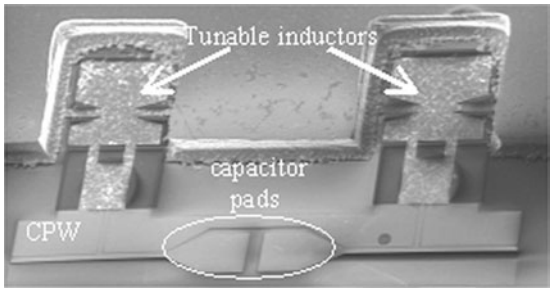

Figure 13. The tunable phase shifter realized (SEM view).

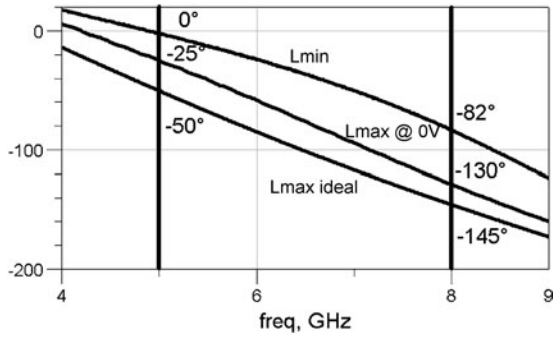

Figure 14. Simulated phase shift for different actuation configurations (including measurement data).

composed of two parallel tunable inductors and one metal–insulator–metal (MIM) constant value capacitor (figure 13). We have also designed a phase shifter in which both the inductors and the MAM capacitor are tunable.

5.2. Simulations

Simulations of the designed phase shifter have been performed using the measurement data-set files of the second tunable inductor from 1 to 15 GHz. The schematic of the system (figure 12) is simulated using *Agilent ADS*, the tunable inductor being replaced by the S_{11} measured parameter for different configurations, and the capacitor by a 1 pF MIM capacitor. We can observe a simulated phase shift of 25° at 5 GHz and 48° at 8 GHz (figure 14). As the inductance variations are continuous, we will measure continuous phase shift, but the real phase shift will be more important than the simulated value, as the simulation includes measurements of the deformed mechanical structure inductor at 0 V actuation. Moreover, this tunable phase shifter is designed using only tunable inductors, consequently the averaging return losses and insertion losses are important due to mismatching problems. Another phase shifter has been designed using two tunable inductors and a tunable MAM capacitor to reduce

mismatching. This system, having a continuous phase shift, could be an alternative to the classical n-bit phase shifters [5, 6].

6. Conclusion

MEMS integrated on silicon wafers, including RF or microwave functions, appear to be very promising for future communication systems. The integration of tunable capacitors and tunable inductors on silicon will offer new possibilities in wideband filter architectures or new matching solutions. This paper outlines the capabilities of MEMS tunable microinductors designed using mechanical displacements changing the magnetic coupling coefficient between circuits. It has been demonstrated that such new structures can reach high variation ratios. First prototypes present 50% inductance variation and the second prototype variation ratio is expected to reach at least 4 over 1 to 10 GHz. Further measurements, at different actuation voltages, have to be performed, first on the second tunable inductor prototype and then on the tunable RF systems: a simple tunable phase shifter (more than 48° phase shift expected at 8 GHz) and a tunable impedance. To reduce the actuation voltage while continuing to increase the variation ratio, we will also consider a new way to realize these structures using polymer materials.

Acknowledgments

The authors wish to acknowledge the assistance and support of L Rousseau, F Marty, research engineers, and the SMM team during the fabrication process in the ESIEE clean room. This work is supported by the French Department of Defense (DGA).

References

[1] Fischer G, Eckl W and Kaminski G 2003 RF-MEMS and SiC/GaN as enabling technologies for a reconfigurable multi-band/multi-standard radio *Bell Lab. Tech. J.* **7** 169–89

[2] Saleh N 1978 Variable Microelectronic Inductors *IEEE Trans. Compon. Hybrids Manuf. Technol.* **1** 118

[3] Zhou S, Sun X Q and Carr W N 1999 A monolithic variable inductor network using microrelays with combined thermal and electrostatic actuation *J. Micromech. Microeng.* **9** 45–50

[4] Lubecke V, Barber B, Chan E, Lopez D, Gross M and Gammel P 2001 Self-assembling MEMS variable and fixed RF inductors *IEEE Trans. Microw. Theory Tech.* **49** 2093

[5] Tassetti C M, Lissorgues G and Gilles J P 2003 New tunable RF MEMS microinductors design *Proc. MME'03 (Nov. 2003)*

[6] Hung J J, Dussopt L and Rebeiz G M 2003 A low-loss distributed 2-bit W-band MEMS phase shifter *EUMW (Munich, 2003)*

[7] Lee S, Park J H, Kim H T, Kim J M, Kim Y K and Kwon Y 2003 A 15-to 45 GHz low-loss analog reflection-type MEMS phase shifter *2003 IEEE MTT-S International Microwave Symposium Digest*